Chinese Chemical Letters 35 (2024) 109512

Contents lists available at ScienceDirect

Chinese Chemical Letters

journal homepage: www.elsevier.com/locate/cclet

Fluorinated [2]rotaxanes as sensitive ^{19}F MRI agents: Threading for higher sensitivity

Lan Yang[a,c,1], Yu Li[a,1], Mou Jiang[a,b,1], Rui Zhou[a,b], Hengjiang Cong[c], Minghui Yang[a,b], Lei Zhang[a,b], Shenhui Li[a,b], Yunhuang Yang[a,b], Maili Liu[a,b], Xin Zhou[a,b,d], Zhong-Xing Jiang[a,b,*], Shizhen Chen[a,b,d,*]

[a] State Key Laboratory of Magnetic Resonance and Atomic and Molecular Physics, National Center for Magnetic Resonance in Wuhan, Wuhan Institute of Physics and Mathematics, Innovation Academy for Precision Measurement Science and Technology, Chinese Academy of Sciences-Wuhan National Laboratory for Optoelectronics, Wuhan 430071, China
[b] University of Chinese Academy of Sciences, Beijing 100049, China
[c] School of Pharmaceutical Sciences & College of Chemistry and Molecular Sciences, Wuhan University, Wuhan 430071, China
[d] Optics Valley Laboratory, Wuhan 430074, China

ARTICLE INFO

Article history:
Received 23 September 2023
Revised 22 December 2023
Accepted 8 January 2024
Available online 13 January 2024

Keywords:
Rotaxane
^{19}F MRI
Imaging agent
Mechanical bond
Relaxation rate

ABSTRACT

As a promising imaging technology, the low sensitivity of fluorine-19 magnetic resonance imaging (^{19}F MRI) severely hinders its biomedical applications. Herein, we have developed an unprecedented rotaxane-based strategy to improve the sensitivity of ^{19}F MRI agents. By threading the fluorinated macrocycle into 2-blade pinwheel [2]rotaxanes, the ^{19}F longitudinal relaxation rate R_1 was dramatically increased, resulting in a significant ^{19}F MRI signal intensity enhancement of up to 79%. Through comparative molecular dynamics studies using a series of solution and solid-state ^{1}H/^{19}F nuclear magnetic resonance (^{1}H/^{19}F NMR) and molecular dynamics simulations, it was found that the formation of mechanical bonds dramatically restricts the motion of the wheel fluorines and thus increasing the R_1 for higher ^{19}F MRI sensitivity. Besides a novel strategy for improving ^{19}F MRI sensitivity, this study has established ^{19}F NMR/MRI as a valuable technology for monitoring the molecular dynamics of rotaxanes, which may shed new light on high-performance ^{19}F MRI agents and molecular devices.

Among biomedical imaging technologies, ^{19}F MRI stands out as a valuable tracer technology for *in vivo* targets [1–4]. The absence of detectable *in vivo* ^{19}F signals in biological systems allows quantitative and selective "hot spot" imaging of targets without background interference, ionizing radiation, and tissue depth limit [5–7]. Despite its great potential, ^{19}F MRI has not yet reached clinical application due to the lack of sensitive ^{19}F MRI agents [6]. Since ^{19}F signals originate only from ^{19}F MRI agents, a relatively high local ^{19}F concentration of about 5 mmol/L is usually required to generate "hot spot" images within a few minutes of data acquisition. For regular ^{19}F MRI agents with ^{19}F signal splitting and low longitudinal relaxation rates (R_1), even higher ^{19}F concentration and longer data acquisition time are required. For *in vivo* studies, it is very challenging to achieve such high ^{19}F concentrations and to keep the animals alive and still for a long time. Therefore, there is an urgent need for highly sensitive imaging agents to reduce the ^{19}F MRI agent dosage and shorten the data acquisition time.

Two major strategies have been developed to improve the sensitivity of ^{19}F MRI agents. First, the assembly of multiple equivalent fluorines can avoid ^{19}F signal splitting and generate a unified strong signal for ^{19}F MRI. Perfluoro–*tert*-butanol derivatives [8], perfluoro-15-crown-5 [9], and perfluoropolyethers [10] are among the most successful ones. However, the more equivalent fluorines require the more complicated synthesis and the higher cost. Second, extending the ^{19}F R_1 can significantly shorten the data acquisition time and acquire more ^{19}F signals in a given time. Many methods have been established to extend the ^{19}F R_1, such as the introduction of paramagnetic metal ions [11,12], conjugation to large molecules [13], self-assembly into aggregates [14,15]. However, these strategies are often hampered by the delicate design and tedious synthesis, the toxicity of paramagnetic metal ions, the ^{19}F signal quenching by the severely extended transverse relaxation rate (R_2), *etc*. Thus, developing novel strategies to extend the ^{19}F R_1 of metal-free agents with multiple equivalent fluorines may yield highly sensitive ^{19}F MRI agents.

* Corresponding authors.
E-mail addresses: zxjiang@apm.ac.cn (Z.-X. Jiang), chenshizhen@apm.ac.cn (S. Chen).
[1] These authors contributed equally to this work.

https://doi.org/10.1016/j.cclet.2024.109512
1001-8417/

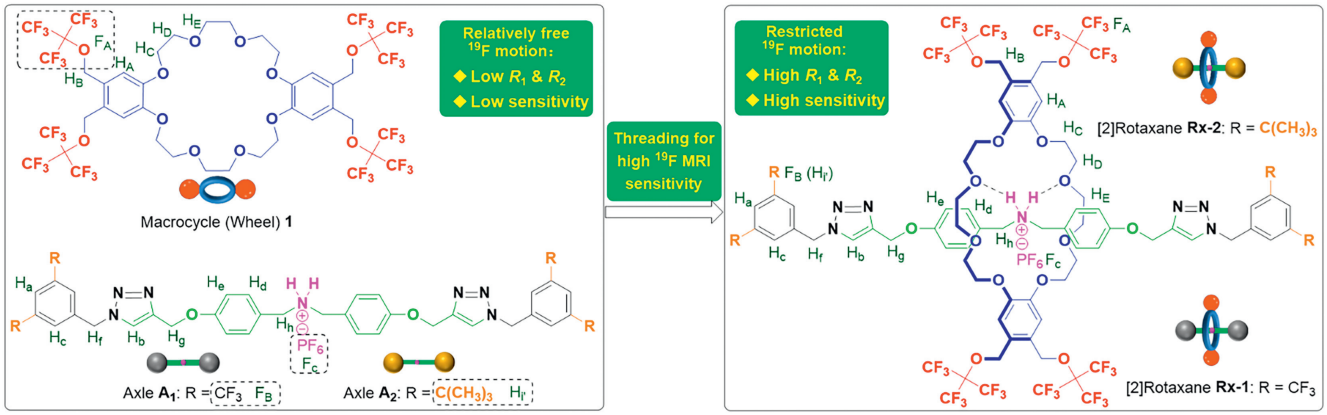

Scheme 1. The strategy of improving ^{19}F MRI agent sensitivity by threading the macrocycle **1** into [2]rotaxanes **Rx-1** and **Rx-2**.

[2]Rotaxanes [16–19], a class of interlocked molecules, have recently attracted our attention. Compared to the relatively free motion of wheel molecules, their motion in [2]rotaxanes is restricted to mechanical bond-guided shuttling and tumbling [20–22]. Although, to our knowledge, the relaxation behavior of rotaxanes has never been investigated, it is reasonable to predict that the R_1 and R_2 of the wheel fluorines can be significantly extended after threading into [2]rotaxanes, resulting in a significant improvement in ^{19}F MRI sensitivity. To validate this novel strategy for improving ^{19}F MRI agent sensitivity, we have herein designed 2-blade pinwheel [2]rotaxanes **Rx-1** and **Rx-2** as sensitive ^{19}F MRI agents and investigated the role of the threading in modulating the motion of wheel fluorines (Scheme 1). With 36 equivalent fluorines to generate a unified strong ^{19}F signal for ^{19}F MRI, fluorinated macrocycle **1** was used both as a regular ^{19}F MRI agent and as the wheel of [2]rotaxanes. Since the ^{19}F R_1 and R_2 are strongly influenced by molecular dynamics, the fluorines act not only as ^{19}F MRI signal sources but also as sensitive status reporters, providing an unprecedented strategy to investigate the mechanical bond and molecular dynamics of [2]rotaxanes, which is a very important and challenging task for rotaxanes [23–25].

First, we prepared macrocycle **1** through a bromomethylation-perfluoro–*tert*-butoxylation strategy, which was then supramolecularly assembled into **Rx-1** and **Rx-2** through a one-pot thread-cap strategy on multi-hundred-milligram scales (see Supporting information for details) [26]. Despite its bulky size, the 4 perfluoro–*tert*–butyl groups at the far end of **1** did not hinder the threading and the [2]rotaxanes were conveniently prepared in good yields. Meanwhile, capped axles $\mathbf{A_1}$ and $\mathbf{A_2}$ were also prepared as reference standards.

Subsequently, 1D and 2D ^{1}H NMR were used to verify the formation of **Rx-1** and **Rx-2**. By comparing the ^{1}H NMR spectra, the typical chemical shift changes ($\Delta\delta$) of the corresponding protons confirmed the formation of the [2]rotaxanes (Figs. 1a-e). Compared with axle $\mathbf{A_1}$, the downfield shift of proton H_h in **Rx-1** indicated the formation of hydrogen bonds between the crown ether and the positively charged amine, while the upfield shifts of protons H_A, $H_{e,}$ and H_g indicated π-π stacking of the wheel and axle aromatic groups. Similar chemical shift changes were also observed in the ^{1}H NMR spectrum of **Rx-2**. Furthermore, the stationing of the wheel in both [2]rotaxanes was verified by the appearance of cross-peaks between wheel protons H_C, H_D, H_E and axle protons H_d, H_h, $H_{c'}$, $H_{h'}$ in their 2D ROESY ^{1}H NMR spectra (Fig. 1g and Fig. S1 in Supporting information). To investigate the "shuttling" motion of the wheel, we removed the hydrogen bonds in the [2]rotaxanes with sodium hydroxide. However, considerable free **1** was detected in the reaction mixture of **Rx-1**, suggesting that the 3,5-bis(trifluoromethyl) benzyl group was not bulky enough to lock **1**. The bulkier 3,5-di–*tert*-butylbenzyl group successfully locked **1** and provided **Rx-2′**. The complicated ^{1}H NMR spectrum of **Rx-2′**showed that the wheel "shuttled" from the central amine to one of the triazole groups and the corresponding protons on either side became non-equivalent (Figs. 1d and f). For example, the *tert*–butyl protons $H_{i'}$ split into two equivalent peaks at 1.27 ppm ($H_{ia'}$) and 1.24 ppm ($H_{ib'}$, see Supporting information for details). The upfield shifts of protons H_E, $H_{c'}$, $H_{h'}$ and the downfield shifts of protons $H_{a'}$, $H_{g'}$ suggest that the "shuttling" is probably driven by the π-π interaction between the wheel benzene and the axle triazole.

Furthermore, we obtained the single-crystal X-ray structure of **1** and discovered a "wide open" conformation (Fig. 1h), providing enough space for the threading. Consistent with the ^{1}H NMR results, the single-crystal X-ray structure of **Rx-1** showed the hydrogen bonds between the wheel and the axle (dotted lines in Fig. 1i) and an "open" conformation of the wheel to accommodate the axle. The X-ray data also showed the π-π stacking between the wheel and the axle, with the distances between adjacent aromatic groups about 0.36–0.40 nm. Notably, the mechanical bond, hydrogen bonds, and π-π stacking in **Rx-1** resulted in a twisted "Z" conformation of the wheel and a broad "W" conformation of the axle.

Meanwhile, ^{19}F NMR was employed to investigate the structure of the [2]rotaxanes (Figs. 1j-n). As designed, the 36 wheel fluorines in **Rx-1** and **Rx-2** gave a unified sharp ^{19}F peak at −71.3 ppm (F_A, Figs. 1l and m), while the 12 axle fluorines in **Rx-1** gave another unified sharp ^{19}F peak at −64.0 ppm (F_B, Fig. 1l). The unified ^{19}F peaks indicate the rapidly interchangeable and equivalent positions of the fluorines, even though the X-ray structure of **Rx-1** shows an unsymmetrical conformation with a crowded π-π stacking side and a loose side. Furthermore, the similar ^{19}F diffusion coefficients (D) of the wheel (F_A: $D = 8.75 \times 10^{-10}$ m^2/s) and the axle (F_B: $D = 8.74 \times 10^{-10}$ m^2/s) in **Rx-1** suggest their synchronous motion as a whole molecule (Table S1 in Supporting information). Compared to **1** (F_A: $D = 1.17 \times 10^{-9}$ m^2/s) and axle $\mathbf{A_1}$ (F_B: $D = 1.14 \times 10^{-9}$ m^2/s), the threading was accompanied by a significant decrease in diffusion coefficients (F_A: 25% reduction, F_B: 23% reduction) as a result of forming a larger molecule.

After elucidating the [2]rotaxane structures, we comparatively studied the effect of the threading on relaxation rates (R). Compared to **1**, the [2]rotaxanes showed similar relaxation rate changes (ΔR) in wheel fluorines F_A (**Rx-1**: $\Delta R_1 = 30\%$, $\Delta R_2 = 40\%$; **Rx-2**: $\Delta R_1 = 28\%$, $\Delta R_2 = 38\%$, Fig. 2a), indicating that the motion of F_A was significantly restricted by the threading. Meanwhile, compared to $\mathbf{A_1}$ and $\mathbf{A_2}$, the [2]rotaxanes showed similar ΔR in axle fluorines F_B (**Rx-1**: $\Delta R_1 = 8\%$, $\Delta R_2 = 9\%$) and protons $H_{i'}$ (**Rx-2**: $\Delta R_1 = 13\%$, $\Delta R_2 = 11\%$, Fig. 2b). Notably, the threading resulted in less ΔR in axle fluorines, suggesting that the axle motion is less constrained by the threading. We also investigated the effect of hydrogen

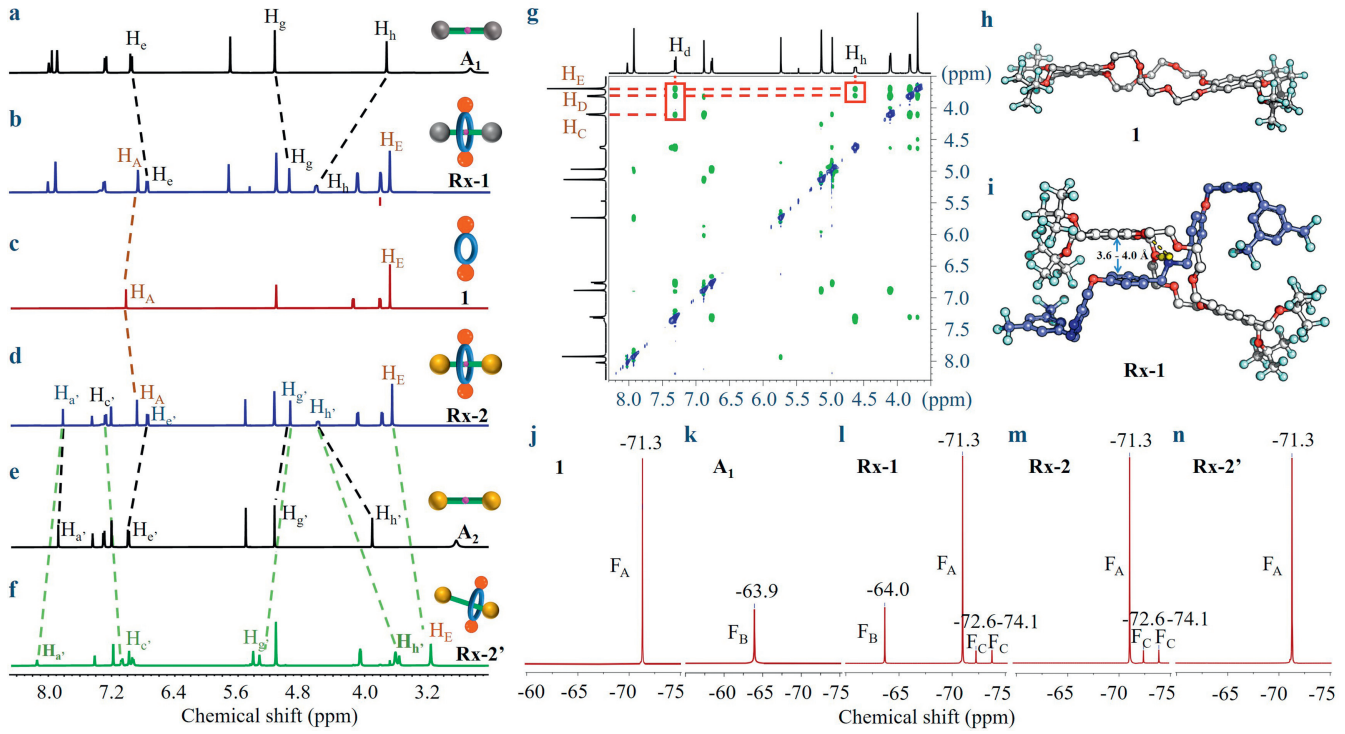

Fig. 1. Partial ^{1}H NMR spectra of the axles, macrocycle, and [2]rotaxanes (a-f); 2D ROESY ^{1}H NMR spectrum of **Rx-1** (g); single-crystal X-ray structure of **1** (h) and **Rx-1** (i); partial ^{19}F NMR spectra of **1** (j), **A$_1$** (k), **Rx-1** (l), **Rx-2** (m), **Rx-2′** (n). NMR conditions: 500 MHz, 1 mmol/L, 298 K, CD_3CN. The labeling of ^{1}H and ^{19}F can be found in Scheme 1 and Scheme S2 (Supporting information).

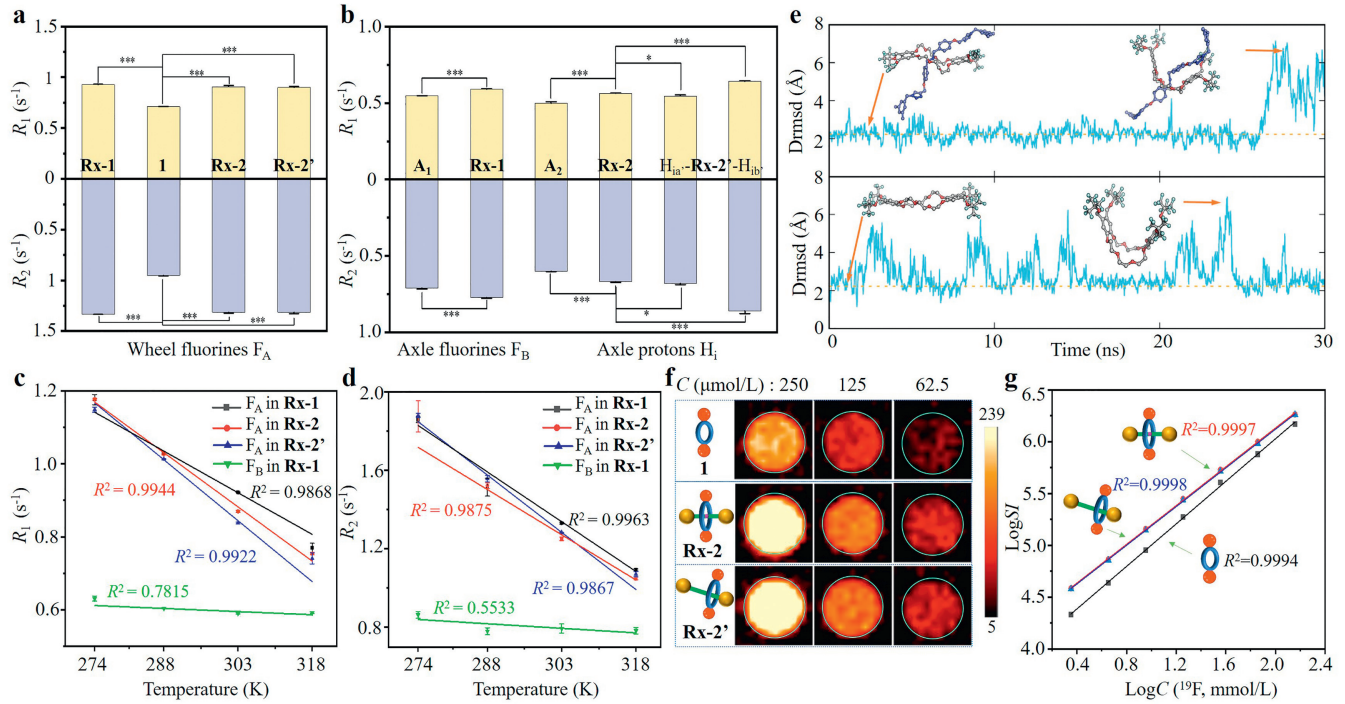

Fig. 2. R_1/R_2 of F_A (a), F_B and H_i (b) in the axles, macrocycle, and [2]rotaxanes; temperature-dependent ^{19}F R_1 (c) and R_2 (d) of the [2]rotaxanes. Drmsd of **Rx-1** (upper) and **1** (lower) over time (e), (f) ^{19}F MRI phantom images (9.4 T, 298 K, CH_3CN) and the plot of logSI *versus* log*C*(^{19}F) (g) of **1**, **Rx-2** and **Rx-2′**. Statistical significance: $^{*}P < 0.1$ and $^{***}P < 0.001$.

bonds and molecular weight on the F_A *R*. Surprisingly, **Rx-2′**with no hydrogen bond and lower molecular weight gave almost identical F_A *R* as **Rx-2** (Fig. 2a), illustrating their minor influence on the wheel motion. Interestingly, opposite ΔR was observed in the *tert*–butyl protons of **Rx-2′**, *i.e.*, substantial increases on the wheel side ($H_{ib'}$: $\Delta R_1 = 14\%$, $\Delta R_2 = 28\%$) and slight changes on the other side ($H_{ia'}$: $\Delta R_1 = -3\%$, $\Delta R_2 = 2\%$, Fig. 2b). These observations show that the threading can efficiently improve the ^{19}F relaxation rates of the wheel, in which the mechanical bond dominantly constrains the motion of the fluorines and protons in a distance-dependent manner. Since molecular motion is closely related to temperature, the impact of temperature on the relaxation rates was investigated

(Figs. 2c and d). Upon heating the [2]rotaxanes from 274 K to 318 K, the wheel fluorines F_A *R* decreased significantly in a similar trend ($\Delta R_1 \approx -35\%$, $\Delta R_2 \approx -43\%$), whereas those of axle fluorines F_B decreased only slightly ($\Delta R_1 = -6\%$, $\Delta R_2 = -9\%$), showing that heating promotes the motion of the wheel much more than that of the axle, probably due to the distance-dependent effect of the mechanical bond. It is noteworthy that the perfect proportional relationship between wheel ^{19}F *R* and temperature makes the [2]rotaxanes valuable temperature probes.

To investigate the origin of the ΔR, molecular dynamics simulations were performed on **1** and **Rx-1**. The simulations showed that the distance root-mean-square deviation (Drmsd) of wheel fluorines F_A relative to the X-ray structure of **1** changed rapidly and significantly over time (Fig. 2e), indicating that F_A underwent rapid and intense motion. In contrast, the Drmsd of $\mathbf{F_A}$ in **Rx-1** changed much slower and smaller, suggesting that the motion of F_A was significantly constrained after the threading. Therefore, the ^{19}F ΔR is probably a result of the wheel motion restricted by the mechanical bond.

In addition, solid-state ^{19}F magic angle spinning (MAS) NMR was performed on **1** and **Rx-2** (Fig. S7 in Supporting information) to obtain the rotational correlation time (τ_c), which is an important parameter characterizing the internal rotations of a given group [27]. It was found that the τ_c of **Rx-2** is about 2.2-fold longer than that of **1** (Fig. S8 in Supporting information), indicating that the rotation of F_A in **Rx-2** is significantly restricted by the threading. In addition, the broader ^{13}C NMR linewidth in **Rx-2** than that of **1** further confirms the slower rotational motion of F_A in **Rx-2** (Fig. S9 in Supporting information). Thus, the rotational motions of wheel fluorines F_A were severely restricted by the threading, resulting in a significant ΔR.

With the significantly increased R_1 and a unified ^{19}F signal from 36 fluorines, the ^{19}F MRI capability of **Rx-2** and **Rx-2′** was evaluated. For ^{19}F MRI agents, short longitudinal relaxation times (T_1, $T_1 = 1/R_1$) and high T_2/T_1 ratios ($T_2 = 1/R_2$) are highly preferred to improve sensitivity by providing an intense ^{19}F peak for rapid data acquisition [28]. The significantly reduced T_1 and high T_2/T_1 ratios of 0.69 establish **Rx-2** and **Rx-2′** as valuable ^{19}F MRI agents. Using the T_1-weighted ^{19}F MRI, **Rx-2** and **Rx-2′** generated high contrast "hot spot" images with a short data acquisition time of 307 s at a low concentration of 62.5 μmol/L (Fig. 2f), which is beyond the reach of most ^{19}F MRI agents. For instance, previous studies have reported the ^{19}F MRI of perfluorinated erlotinib and gefitinib analogues at concentrations as low as 10 mmol/L [29]. Additionally, a fluorinated peptide with the lowest detectable concentration for ^{19}F MRI was reported to be 0.13 mmol/L [30]. As expected, threading **1** into **Rx-2** and **Rx-2′** significantly improved the ^{19}F MRI sensitivity with 77%−79% signal intensity (SI) enhancement. Notably, the SI enhancement is more significant over the range of *in vivo* drug concentrations, making the [2]rotaxanes highly sensitive ^{19}F MRI agents for potential *in vivo* applications. In each case, the logarithm of SI is proportional to the logarithm of fluorine concentration (Fig. 2g), facilitating quantitative ^{19}F MRI. Since mechanical bond and hydrogen bond are formed during the threading, their effects were detected by the SI enhancement, *i.e.*, mechanical bond and hydrogen bond induced 33% SI enhancement in **Rx-2** and mechanical bond induced 29% SI enhancement in **Rx-2′**. Therefore, introducing mechanical bonds is an effective and robust strategy to improve ^{19}F MRI sensitivity.

In conclusion, we have developed a novel strategy to improve the sensitivity of ^{19}F MRI agents. On the one hand, the introduction of mechanical bond into ^{19}F MRI agents has been demonstrated to restrict the motion of the fluorines, shorten the T_1, maintain high T_2/T_1 ratios, and thus dramatically improve the sensitivity, providing a novel strategy to address the sensitivity issue of ^{19}F MRI. On the other hand, fluorinated rotaxanes are rare and their potential in ^{19}F MRI has never been explored. We have unprecedentedly synthesized a series of fluorinated 2-blade pinwheel [2]rotaxanes and employed ^{19}F NMR/MRI to investigate the structure and molecular dynamics of [2]rotaxanes, establishing ^{19}F NMR/MRI as a valuable technology for sensing mechanical bonds in molecular devices. This study successfully integrated ^{19}F MRI and rotaxanes, which may promote the development of highly sensitive and stimuli-responsive ^{19}F MRI agents, such as temperature probes, and self-status-reporting high-performance molecular devices.

Declaration of competing interest

The authors declare that they have no known competing financial interests or personal relationships that could have appeared to influence the work reported in this paper.

Acknowledgments

This work was supported by the Strategic Priority Research Program of the Chinese Academy of Sciences (No. XDB0540000), the National Key R&D Program of China (No. 2018YFA0704000), the National Natural Science Foundation of China (Nos. 22327901, 22077098, U21A20392, 21921004, and 82127802), and the Knowledge Innovation Program of Wuhan-Basic Research (No. 2022020801010137). Shizhen Chen acknowledges the support from the Youth Innovation Promotion Association and the Young Top-notch Talent Cultivation Program.

Supplementary materials

Supplementary material associated with this article can be found, in the online version, at doi:10.1016/j.cclet.2024.109512.

References

[1] M. Higuchi, N. Iwata, Y. Matsuba, et al., Nat. Neurosci. 8 (2005) 527–533.
[2] M.J. Couch, I.K. Ball, T. Li, et al., Magn. Reson. Imaging 49 (2019) 343–354.
[3] P. Bouvain, S. Temme, U. Flögel, WIREs Nanomed. Nanobiotechnol. 12 (2020) e1639.
[4] H. Lin, X. Tang, A. Li, J. Gao, Adv. Mater. 33 (2021) 2005657.
[5] S. Kunjachan, J. Ehling, G. Storm, F. Kiessling, T. Lammers, Chem. Rev. 115 (2015) 10907–10937.
[6] I. Tirotta, V. Dichiarante, C. Pigliacelli, et al., Chem. Rev. 115 (2015) 1106–1129.
[7] J. Ruiz-Cabello, B.P. Barnett, P.A. Bottomley, J.W.M. Bulte, NMR Biomed. 24 (2011) 114–129.
[8] T. Wu, A. Li, K. Chen, et al., Chem. Commun. 57 (2021) 7743–7757.
[9] L. Mignion, J. Magat, O. Schakman, et al., Magn. Reson. Med. 69 (2013) 248–254.
[10] E.T. Ahrens, R. Flores, H. Xu, P.A. Morel, Nat. Biotechnol. 23 (2005) 983–987.
[11] D. Xie, M. Yu, R.T. Kadakia, E.L. Que, Acc. Chem. Res. 53 (2020) 2–10.
[12] K.H. Chalmers, E. DeLuca, N.H.M. Hogg, et al., Chem. Eur. J. 16 (2010) 134–148.
[13] L. Zhu, Y. Li, M. Jiang, et al., ACS Appl. Mater. Interfaces 15 (2023) 2665–2678.
[14] A.T. Preslar, F. Tantakitti, K. Park, et al., ACS Nano 10 (2016) 7376–7384.
[15] Y. Takaoka, T. Sakamoto, S. Tsukiji, et al., Nat. Chem. 1 (2009) 557–561.
[16] P.L. Anelli, P.R. Ashton, R. Ballardini, et al., J. Am. Chem. Soc. 114 (1992) 193–218.
[17] C.A. Schalley, K. Beizai, F. Vögtle, Acc. Chem. Res. 34 (2001) 465–476.
[18] B. Zheng, M. Zhang, S. Dong, X. Yan, M. Xue, Org. Lett. 15 (2013) 3538–3541.
[19] B.L. Feringa, Angew. Chem. Int. Ed. 56 (2017) 11060–11078.
[20] R.E. Fadler, A.H. Flood, Front. Chem. 10 (2022) 856173.
[21] G. Gholami, K. Zhu, G. Baggi, et al., Chem. Sci. 8 (2017) 7718–7723.
[22] K. Yamauchi, A. Miyawaki, Y. Takashima, H. Yamaguchi, A. Harada, J. Org. Chem. 75 (2010) 1040–1046.
[23] Y.F. Yin, M.Y. Yun, L. Wu, et al., Angew. Chem. Int. Ed. 58 (2019) 12705–12710.
[24] A. Garci, Y. Beldjoudi, M.S. Kodaimati, et al., J. Am. Chem. Soc. 142 (2020) 7956–7967.
[25] P. Rajamalli, F. Rizzi, W. Li, et al., Angew. Chem. Int. Ed. 60 (2021) 12066–12073.
[26] V. Blanco, A. Carlone, K.D. Hänni, D.A. Leigh, B. Lewandowski, Angew. Chem. Int. Ed. 51 (2012) 5166–5169.
[27] X. Lu, C. Huang, M. Li, et al., J. Phys. Chem. B 124 (2020) 5271–5283.
[28] Y. Mo, C. Huang, C. Liu, et al., Macromol. Rapid Commun. 44 (2023) 2200744.
[29] S.E. Kirberger, S.D. Maltseva, J.C. Manulik, et al., Angew. Chem. Int. Ed. 56 (2017) 6440–6444.
[30] H. Shi, B. Lai, S. Chen, et al., Chin. J. Chem. 35 (2017) 1693–1700.